

The Assembly and Testing of the Spin Dressing Magnet for the Neutron Electric Dipole Experiment

Thesis by
Jessica Fox

In Partial Fulfillment of the Requirements for the
Degree of
BS in Physics

The logo for the California Institute of Technology (Caltech), featuring the word "Caltech" in a bold, orange, sans-serif font.

CALIFORNIA INSTITUTE OF TECHNOLOGY
Pasadena, California

2025
Defended May 27, 2025

© 2025

Jessica Fox

ORCID: 0000-0001-5053-229X

All rights reserved

ACKNOWLEDGEMENTS

I would first like to thank Professor Bradley Filippone for being my research mentor since freshman year and allowing me to continue working in his research group. He has helped me with both the academic and logistical aspects of doing research both on and off campus. I would also like to thank him for the help he gave me when I was applying to graduate school.

I would also like to thank Dr. Alina Aleksandrova and Dr. Marie Blatnik for helping me through my first research experience during my freshman year of college. Without them, I probably would not have had the same experience with research and my path could have been very different.

I would like to thank Raymond Tat and Rhett Alston Crowley for helping me with COMSOL, for without them I would likely have been lost to the learning curve of the software. In addition, I would like to thank Robin Zhu for all of his organization and his help in guiding my work.

Next, I would like to thank my parents and sister for always supporting me no matter what. I would not be where I am today without their support, help, and sacrifices.

I would like to lastly thank all the friends that I have made at Caltech. They have been an incredible support network and the thing I am most sad about leaving upon graduation.

ABSTRACT

The discrepancy between the quantity of matter and antimatter in the universe is something that can likely be attributed to violations in the fundamental symmetries of the universe; however, much like the antimatter itself, there is a discrepancy between the required versus observed magnitude of these violations. One theory states that, to account for these violations in symmetry, the neutron must have an electric dipole moment. One such method to find the existence and magnitude of the neutron electric dipole moment (nEDM) is the critical dressing method. Such a method requires the use of two superconducting magnets with perpendicular magnetic fields. This specific method of critical dressing uses superfluid Helium-4, polarized Helium-3, and ultracold polarized neutrons, with critical dressing occurring when the Helium-3 precession rates are equivalent. This method is used to determine the existence of an nEDM, if there is critical dressing with an electric field, there is no nEDM, but if there is a precession rate difference with the electric field, there is an EDM that can thus be measured. Over the past several months, the assembly of the spin dressing magnet used in the critical dressing portion of the nEDM experiment has begun. This has included assembling the boss rings, constructing the magnet frame, placing the story sticks and wire guides, and winding the superconducting wire around the coil skeleton. Data was also taken using this wire. Furthermore, simulations have been run on COMSOL Multiphysics to compare the theoretical predictions with the measurements of the magnetic field and B-field gradients produced by the spin dressing magnet.

TABLE OF CONTENTS

Acknowledgements	iii
Abstract	iv
Table of Contents	v
List of Illustrations	vi
Chapter I: Introduction	1
Chapter II: Assembling the Spin Dressing Magnet	5
Chapter III: COMSOL Simulation	17
Chapter IV: Testing the Spin Dressing Magnet	24
Chapter V: Future Work with the Magnet	31
Chapter VI: Conclusion	32
Appendix A: Wire Placements	34

LIST OF ILLUSTRATIONS

<i>Number</i>	<i>Page</i>
1.1 A labeled diagram of the entire nEDM apparatus. [4]	3
1.2 A labeled diagram showing how the spin dressing magnet (labeled "dressing coil") fits into the full apparatus. [4]	3
1.3 A labeled diagram of the spin dressing magnet. The labeled parts are the boss rings, the hoops, the gussets, the wire guides, the story sticks, and the lead end caps. Everything labeled in the frame is comprised of G10.	4
2.1 Two images of preconstructed hoops during the process of gluing, in which the pieces are laid out in gluing order (closest to edge of table to center of table). The pieces would then be covered in a thin layer of epoxy glue and attached together, before being covered in cling wrap and vacuum sealed while the epoxy cured. Visible in each image are a series of rectangular slots along the inner curve of the hoops, which are where the wire guides go.	6
2.2 The leftmost image shows the table on which the rings are placed for measurement without the ring. The raised metal ring acts as a brace for the hoop or boss ring and is reversible depending on if a ring or a hoop is being measured, and it holds the ring or hoop in place. The rightmost image is of the same table, but with a ring placed on the table, showing how the rings fit into the brace. This table is also where the gluing has taken place.	7
2.3 These two images show the rings for the spin dressing magnet placed (both uncovered, as in the leftmost image, and covered, as in rightmost image) in the cryotesting container. The rings are propped up on on styrofoam in a styrofoam and wood container lined with plastic, and a small temperature probe is attached to a ring. The container is then covered with more foam and liquid nitrogen is pumped into the container until the minimum possible temperature is reached. The temperature is monitored and the rings are allowed to sit until the liquid nitrogen evaporates.	8

2.4	This image shows the ring in the brace on the table with the ROMER arm in the middle. To take the measurements, one person would be putting the measurement adapter into each slot, as well as ensuring that the correct slot is being measured. The other person must sit on the table and manually move the tip of the romer arm to the adapter in each slot and press the button to take the measurement.	8
2.5	A graph of the discrepancy between the expected angle and the actual angle of the wire slots on the third hoop for the spin dressing magnet. The x-axis is the slot number while the y-axis is the angular discrepancy, in degrees. If the discrepancy is graphed to be between the two red lines, then it is considered to be close enough to the theoretical values to be used in the experiment.	9
2.6	Lead was cut in the general shape of the bottom LEC and covered in epoxy glue. The LEC was later placed on top of the lead and the remainder was trimmed away. The LEC was then covered in plastic and vacuum sealed while the epoxy cured. Proper lead safety precautions were taken during this process, including using coveralls.	10
2.7	The story sticks being cleaned with isopropyl alcohol.	10
2.8	Images of the assembly of the spin dressing magnet frame. At this point in the assembly process, the rings are the only things assembled (left) and are resting on wooden scaffolding. In the right figure, a story stick is being inserted into the slot in the rings.	11
2.9	An image of a story stick with one of two gussets in place.	11
2.10	The frame of the spin dressing magnet, with all the story sticks, gussets, and boss rings and hoops, without any external scaffolding. The gussets are placed diagonally across from each other at the junction between each hoop and story stick, with a gusset on both sides of the story sticks where they meet the boss rings.	12
2.11	All of the wire guides for the spin dressing magnet laid out on the table. The wire guides are similarly made of G10 and are designed to fit into the slots on the inside of the rings and hoops. The lines of sharpie mark where the edges needed to be sanded.	12
2.12	Robin, cleaning the ends of the wire guides with isopropyl alcohol by machine.	13
2.13	The bottom of the wire guide, showing the mechanism by which the wire guide is stabilized.	13

2.14	An image of the finished frame for the spin dressing magnet. The finished frame is all of the pieces of the frame without the wire wound or the wire guide caps.	14
2.15	The wire guide caps, which are pieces of G10 that are slid into the wire guide slots, which cover the ridges in the wire guides that hold the wire and keep it in place.	15
2.16	The author, sitting inside the the spin dressing magnet, while coiling the solder wire and inspecting the kapton tape to ensure it is covering the entire portion of the wire.	15
2.17	The wires along the saddle portion of the magnet. The golden-orange color is from the kapton tape coating the wire to prevent different sections of the wire from coming into contact with each other.	16
3.1	Two images, showing the regular (top) and zoomed in (bottom) coil from the original COMSOL simulation. As shown in the bottom image, there are tiny gaps between the wires making up circular portion of the coil, which made the simulation impossible to run on a reasonable time scale.	18
3.2	An image showing the second iteration of the COMSOL simulation, specifically highlighting the current directionality of the 1 Amp drop-down wires of the cylinder by the blue highlighted lines with the red arrows.	19
3.3	An image of the finished COMSOL simulation, both without (top) and with (bottom) the mesh. Inside the coil is a small box, showing the area over which the simulation matters most.	20
3.4	A graph of the magnetic field in the x-direction with respect to the x-axis coordinates of the magnet, with the x-axis direction shown in Fig. 1.3. The right side of the graph is the edge of the cylinder, at 0.7m, while the left side is the center of the cylinder, at 0m. Though this is only one quarter of the cylinder, it shows half of the x-axis data and, due to the symmetry of the cylinder, it can be concluded that the data from the other half of the cylinder is the data shown reflected across the y-axis. The magnetic field at the center in this direction is 0.213 G (which agrees with the other two measurements), compared to the 0.223 G calculated by Professor Brad Filippone.	21

3.5	A graph of the magnetic field in the x-direction with respect to the y-axis of the magnet, with the direction of the y-axis shown in Fig. 1.3. The center of the magnet is marked by the origin of the graph's x-axis, with a value of .213 Gauss, which agrees with the other two measurements.	22
3.6	A graph of the magnetic field in the x-direction with respect to the z-axis of the magnet, with the direction of the z-axis shown in Fig. 1.3. The center of the magnet is marked by the origin of the graph's x-axis, with a value of .213 Gauss, which agrees with the other two measurements.	23
4.1	A photo of the power supply (top right), as well as the ammeter (top left) and magnetometer readout (middle left) used for taking the data of the magnetic field. The other two devices in the photo are non-functional power supplies.	25
4.2	Two photos, at varying distances, of the magnetometer probe. The zoomed out image also shows some of the experimental setup. Attached to the probe was a short G10 rod to keep the probe balanced.	26
4.3	A photo of the experimental setup, showing the ruler across the x-axis of the spin dressing magnet, with the probe resting on the magnet.	27
4.4	A graph (top) of both the simulated (line) and experimental (dots) data of the magnetic field in the x-direction taken across the x-axis of the spin dressing magnet. The shape of both sets of data are incredibly similar, even though the experimental values are less than the simulated values. The bottom graph shows the data normalized, with a normalization factor of 0.000799, which is close to the 0.05% error from the magnetometer.	28
4.5	A graph (top) of both the simulated (line) and experimental (dots) data of the magnetic field in the x-direction taken across the y-axis of the spin dressing magnet. The shape of both the experimental data is somewhat similar to that of the theorized data, however, there are significant differences. The data may look more similar if data was taken at more regular intervals. The bottom graph shows the data normalized, with a normalization factor of 0.00221, which is farther from the 0.05% error from the magnetometer than the measurements of B_x in the x direction measurement.	29

- 4.6 A graph (top) of both the simulated (line) and experimental (dots) data of the magnetic field in the x-direction taken across the z-axis of the spin dressing magnet. The shape of both sets of data are incredibly similar, with the experimental values also being similar to simulated values. The two plots would also likely look more similar if experimental data was taken at more regular intervals. The bottom graph shows the data normalized, with a normalization factor of 0.00335, which is farther from the 0.05% error from the magnetometer than either the Bx in the x direction or the Bx in the y direction measurements. 30

Chapter 1

INTRODUCTION

One of the most fundamental questions asked by philosophy is "why is there something rather than nothing?" It has been a question asked for thousands of years by the greatest minds of their times and is still asked to this day. The "something" in our universe, the part of our universe with which we interact, is matter. In the known universe, as observed by astronomers, cosmologists, and others, there is a significant preference for matter over antimatter. Specifically, there is a matter-antimatter discrepancy following the Big Bang at a ratio of 10^{-10} . [1] This such asymmetry is not predicted by the Standard Model of Physics, as it is predicted to be much smaller. [1] This asymmetry during baryogenesis, not accounted for in the Standard Model, has multiple theories behind it, one of which is related to violations in the fundamental symmetries of the universe.

There are three separate discrete symmetries of particle interactions, as well as two combinations thereof. The separate fundamental symmetries are charge (C) symmetry, parity (P) symmetry, and time (T) symmetry, while the combinations are charge-parity (CP) and charge-parity-time (CPT) symmetries. These fundamental symmetries state that the laws of physics act the same way on particles regardless of their charge, parity, or motion through time. These symmetries seem intuitive, and seemingly minor differences in particle properties should not change the way the laws of physics act upon them. However, there have been violations of these symmetries, both in and outside the predictions of the standard model. Inside the standard model, there are violations in CP symmetry that are caused by and are accounted for in kaon and neutral B-meson decays. [2,3] However, there need to be more CP violations in the universe than can be accounted for by the kaon and neutral B meson decay in order to account for the matter-antimatter asymmetry. There are believed to be additional sources of CP violations tied to the possible existence of a neutron electric dipole moment. This additional source of CP violations could explain the matter/antimatter asymmetry, and thus this gave rise to the nEDM experiment.

The nEDM experiment has two main methods for measuring the nEDM: the free

precession method and the spin dressing method. For the purpose of this paper, only the spin dressing method will be discussed. The spin dressing method of measuring the nEDM looks at the precession rate of ultracold polarized neutrons relative to the precession rate of polarized Helium-3. Without an EDM, neutrons and Helium-3 would have an identical scintillation rate. However, with an nEDM, the scintillation rate would change, which can be measured. [3]

The spin dressing method uses two magnets with perpendicular magnetic fields to cause the precessions of the ultracold neutrons and the Helium-3. The primary topic of this paper is the construction of one of the magnets, known as the spin dressing magnet. The spin dressing magnet is the magnet that will produce the field perpendicular to the B_0 magnetic field, which is the primary magnet used in the nEDM experiment. The magnet is made of a fiberglass material (G10) and made of multiple parts, as shown in Fig. 1.3, as well as the apparatus as a whole, as shown in Figs. 1.1 and 1.2.

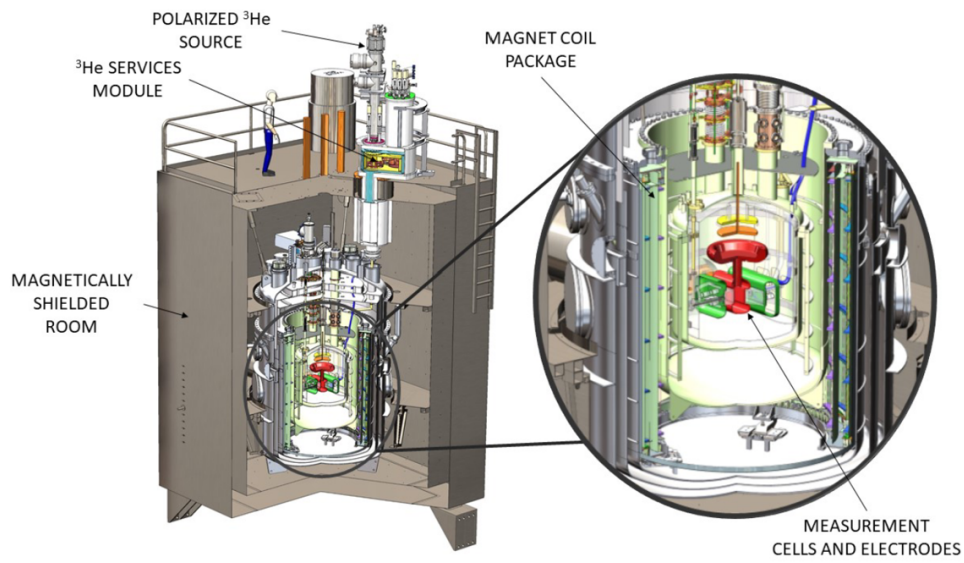


Figure 1.1: A labeled diagram of the entire nEDM apparatus. [4]

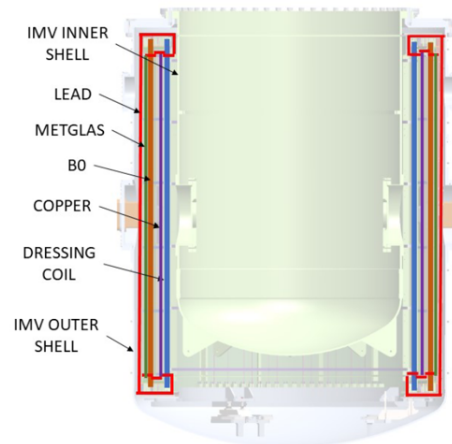


Figure 1.2: A labeled diagram showing how the spin dressing magnet (labeled "dressing coil") fits into the full apparatus. [4]

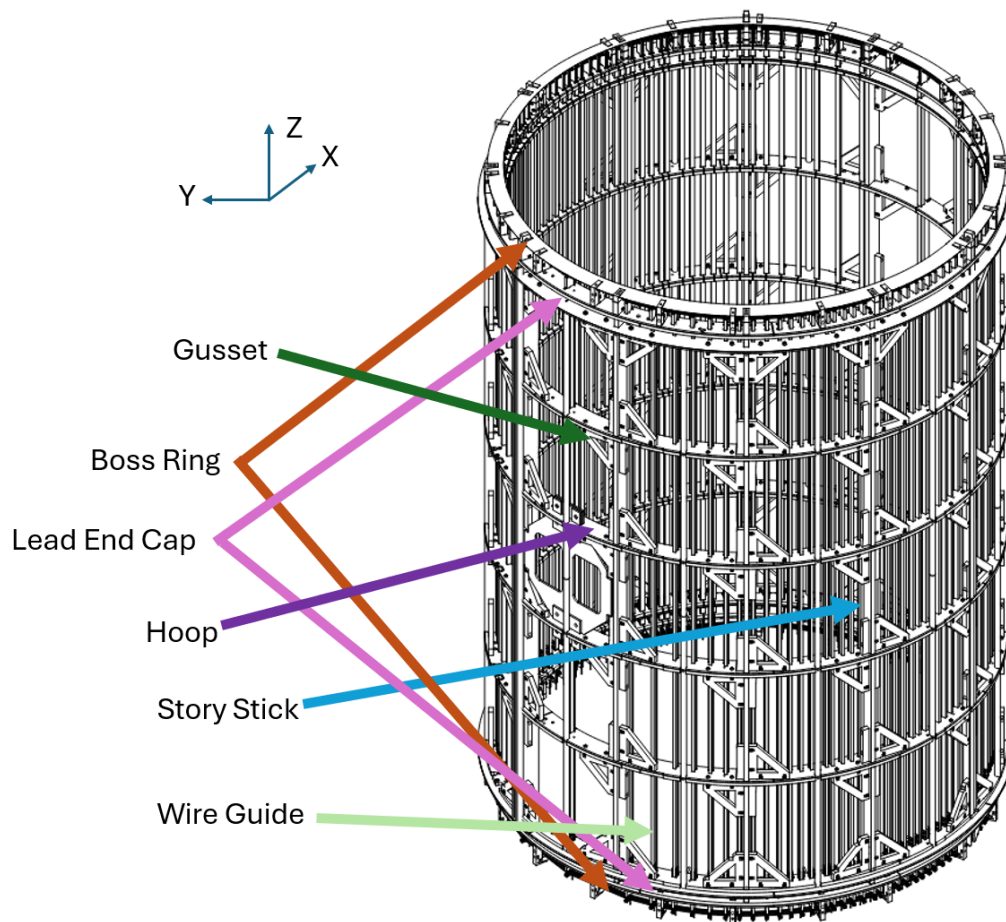


Figure 1.3: A labeled diagram of the spin dressing magnet. The labeled parts are the boss rings, the hoops, the gussets, the wire guides, the story sticks, and the lead end caps. Everything labeled in the frame is comprised of G10.

Chapter 2

ASSEMBLING THE SPIN DRESSING MAGNET

2.1: Assembling Boss Rings and Hoops

The first part of the assembly for the spin dressing magnet was the assembly of the boss rings and hoops. The boss rings are the top and bottom rings of the frame of the spin dressing magnet, while the hoops are the inner four rings. The rings and hoops, as the rest of the frame, are comprised of G10, which is a fiberglass composite layered with epoxy. G10 was chosen as the material for the spin dressing magnet frame, as it is a sturdy material with a low thermal expansion coefficient, meaning that it can both withstand its own weight (as well as the weight of the wires), and it will not contract when cooled to ultra-cold temperatures. Furthermore, G10 is nonferromagnetic and thus will not interfere with the very sensitive magnetic field produced in the spin dressing magnet. [3] The boss rings and hoops were machined in multiple pieces due to the large sizes of the material needed, as shown in Fig. 2.1, with the pieces attached together using epoxy glue and vacuum lamination, which was done on the table shown in Fig. 2.2. For the gluing process, as well as most of the rest of the assembly process, nitrile gloves were worn to protect the skin from chemicals such as epoxy and isopropyl alcohol, as well as to protect G10 from the skin.

Once assembled, the rings and hoops needed to be measured and cold tested. In each ring and hoop, there are small slots, as shown in Fig. 2.1. These slots hold the wire guides, which, in turn, hold the wires. The position of these slots needs to be measured relative to their expected position both before and after being submerged in liquid nitrogen (Fig. 2.3) to measure any thermal effects on the G10 (that is, to ensure no thermal contraction and expansion, as well as to make sure that it will not break when the magnet is later supercooled). The rings were then returned to the table shown in Fig. 2.2, and the position of these slots was measured with the ROMER arm (Fig. 2.4), which recorded the position of each slot relative to a predefined position. Once the data was collected, it was compared with the expected position of the slots (Fig. 2.5). So long as the difference between the theoretical and actual positions was graphed to be between the two red lines, the

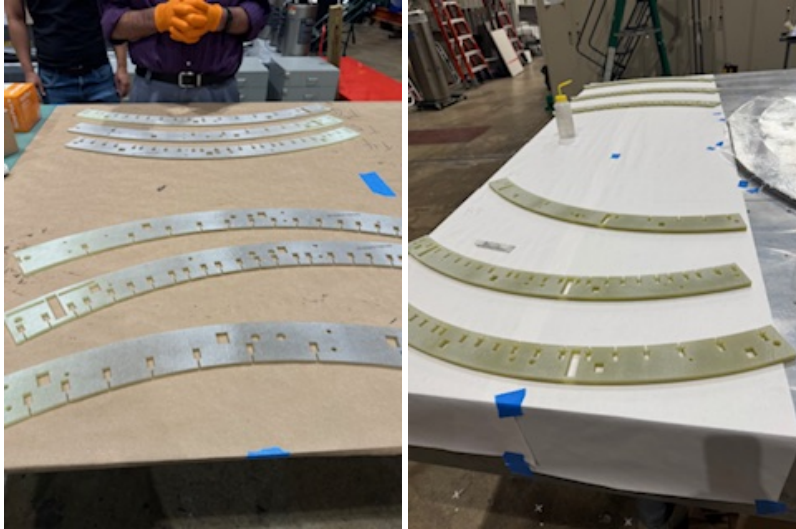


Figure 2.1: Two images of preconstructed hoops during the process of gluing, in which the pieces are laid out in gluing order (closest to edge of table to center of table). The pieces would then be covered in a thin layer of epoxy glue and attached together, before being covered in cling wrap and vacuum sealed while the epoxy cured. Visible in each image are a series of rectangular slots along the inner curve of the hoops, which are where the wire guides go.

discrepancy was deemed to be acceptable, and the ring or hoop was able to be used.

A set of G10 rings, known as lead end caps, or LECs, was attached to a thin layer of lead. (Fig. 2.6) The purpose of the lead is to provide additional superconducting shielding for the magnet. The lead was cut with proper safety precautions and glued to the boss rings using the same epoxy glue used to keep the boss rings and hoops together. These end caps would later be placed at the top and bottom of the spin dressing magnet frame.

2.2: Placing in the Story Sticks and Aligning the Structure

Once the boss rings and hoops were finished, the rings and hoops needed to be assembled to make the skeletal structure of the spin dressing magnet. A wooden scaffold was put in place to provide a structure on which the rings and hoops could rest until the supports were put in place. (Fig. 2.8) The primary vertical supports are known as story sticks and are also made of G10. The rings and hoops, after being placed on the support, had the story sticks slotted into place, and the external supports were removed. Once the story sticks were in place, gussets, which are pieces of G10 shaped like the number “4”, were placed at the corners between the

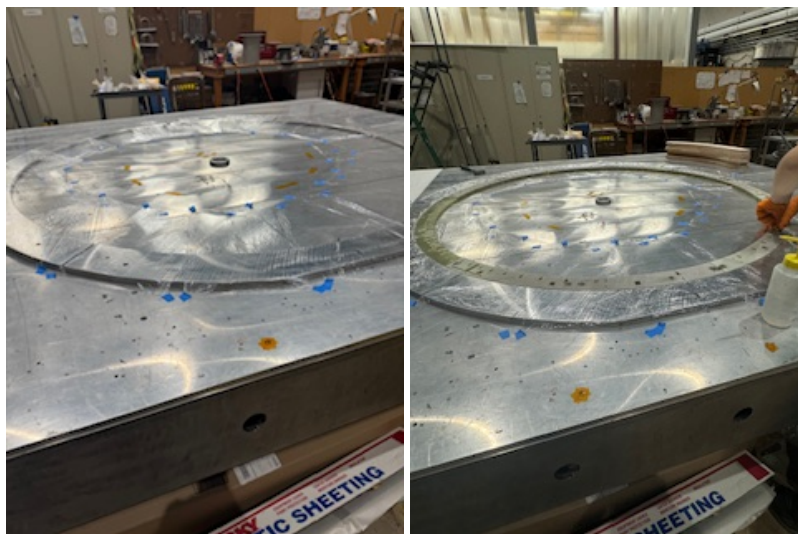


Figure 2.2: The leftmost image shows the table on which the rings are placed for measurement without the ring. The raised metal ring acts as a brace for the hoop or boss ring and is reversible depending on if a ring or a hoop is being measured, and it holds the ring or hoop in place. The rightmost image is of the same table, but with a ring placed on the table, showing how the rings fit into the brace. This table is also where the gluing has taken place.

story sticks and the rings and hoops to provide additional support, as shown in Fig. 2.9 and Fig. 2.10.

Once the story sticks and gussets were in place, the alignment of the spin dressing magnet frame was tested. We used a two-dimensional laser alignment tool to test to see if the frame had any tilting or buckling under its own weight. We aligned one axis of the laser tool with a hoop and the other axis with a wire guide slot, checking to make sure that the wire guide slot lined up with the laser for each ring and hoop. Due to a misalignment of the table, it took longer than expected to test the alignment of the frame of the spin dressing magnet, and it needed to be transferred to a different surface to properly take the measurement.



Figure 2.3: These two images show the rings for the spin dressing magnet placed (both uncovered, as in the leftmost image, and covered, as in rightmost image) in the cryotesting container. The rings are propped up on on styrofoam in a styrofoam and wood container lined with plastic, and a small temperature probe is attached to a ring. The container is then covered with more foam and liquid nitrogen is pumped into the container until the minimum possible temperature is reached. The temperature is monitored and the rings are allowed to sit until the liquid nitrogen evaporates.



Figure 2.4: This image shows the ring in the brace on the table with the ROMER arm in the middle. To take the measurements, one person would be putting the measurement adapter into each slot, as well as ensuring that the correct slot is being measured. The other person must sit on the table and manually move the tip of the romer arm to the adapter in each slot and press the button to take the measurement.

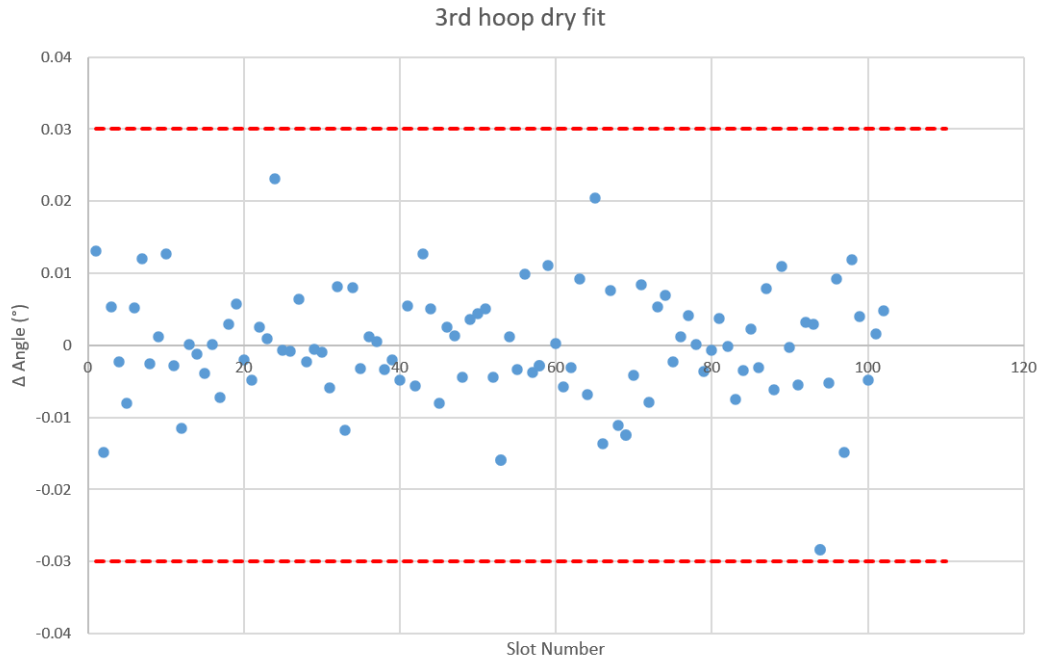


Figure 2.5: A graph of the discrepancy between the expected angle and the actual angle of the wire slots on the third hoop for the spin dressing magnet. The x-axis is the slot number while the y-axis is the angular discrepancy, in degrees. If the discrepancy is graphed to be between the two red lines, then it is considered to be close enough to the theoretical values to be used in the experiment.

2.3: Placing the Wire Guides

Before placing the wire guides (Fig. 2.11) in the frame of the spin dressing magnet, they needed to be properly prepared. To prepare the guides, the edges were sanded at an angle in certain places to prevent any stress on the wire. The guides were then cleaned with isopropyl alcohol, both by hand and by machine (Fig. 2.12), and then placed through the slots in the boss rings and hoops. Each wire guide was then fastened to place at the bottom by an additional piece of G10, as shown in Fig. 2.13. A trial of placing the wire guides was done prior to the official placing of the wire guides as part of the testing process, and, for wire guides near the story sticks, smaller tools and different screws needed to be used, as the human hand would not fit in the allotted space. The completed frame is shown in Fig. 2.14.



Figure 2.6: Lead was cut in the general shape of the bottom LEC and covered in epoxy glue. The LEC was later placed on top of the lead and the remainder was trimmed away. The LEC was then covered in plastic and vacuum sealed while the epoxy cured. Proper lead safety precautions were taken during this process, including using coveralls.



Figure 2.7: The story sticks being cleaned with isopropyl alcohol.

2.4: Coiling the Wire

The wire for the spin dressing magnet is a 50% tin 50% lead solder that is .062 inches thick. It is wound such that a $\cos(\theta)$ coil is created. The coil was wound by hand, with one person inside the coil to move the solder and one person at the top and one person at the bottom of the coil to help tape the wire. The author, sitting inside the magnet, helping to coil the wire, is shown in Fig. 2.16. The wire on the



Figure 2.8: Images of the assembly of the spin dressing magnet frame. At this point in the assembly process, the rings are the only things assembled (left) and are resting on wooden scaffolding. In the right figure, a story stick is being inserted into the slot in the rings.



Figure 2.9: An image of a story stick with one of two gussets in place.

saddle portion of the coil was taped with kapton tape to prevent different portions of the wire from touching each other (as shown in Fig. 2.17), and the vertical portion of the wire is locked in place with a cover shown in Fig. 2.15.

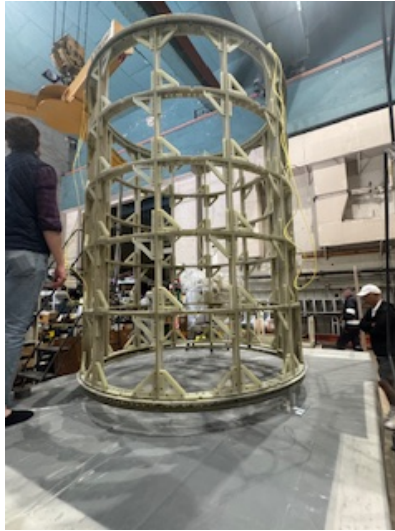


Figure 2.10: The frame of the spin dressing magnet, with all the story sticks, gussets, and boss rings and hoops, without any external scaffolding. The gussets are placed diagonally across from each other at the junction between each hoop and story stick, with a gusset on both sides of the story sticks where they meet the boss rings.

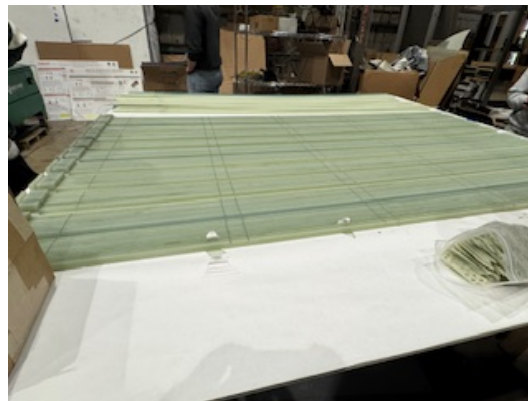


Figure 2.11: All of the wire guides for the spin dressing magnet laid out on the table. The wire guides are similarly made of G10 and are designed to fit into the slots on the inside of the rings and hoops. The lines of sharpie mark where the edges needed to be sanded.

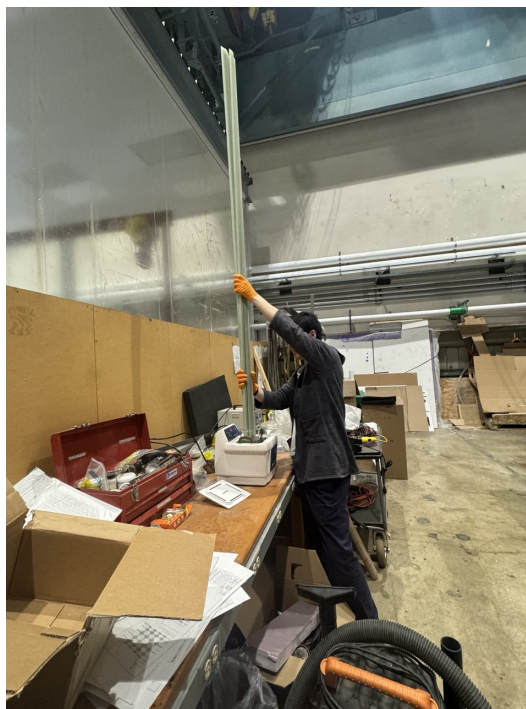


Figure 2.12: Robin, cleaning the ends of the wire guides with isopropyl alcohol by machine.



Figure 2.13: The bottom of the wire guide, showing the mechanism by which the wire guide is stabilized.



Figure 2.14: An image of the finished frame for the spin dressing magnet. The finished frame is all of the pieces of the frame without the wire wound or the wire guide caps.



Figure 2.15: The wire guide caps, which are pieces of G10 that are slid into the wire guide slots, which cover the ridges in the wire guides that hold the wire and keep it in place.



Figure 2.16: The author, sitting inside the the spin dressing magnet, while coiling the solder wire and inspecting the kapton tape to ensure it is covering the entire portion of the wire.



Figure 2.17: The wires along the saddle portion of the magnet. The golden-orange color is from the kapton tape coating the wire to prevent different sections of the wire from coming into contact with each other.

Chapter 3

COMSOL SIMULATION

The most difficult part of the past year of this research that I have had to deal with was the simulation of the spin dressing coil in the COMSOL Multiphysics software. Over the course of several months, from January to May, there have been issues with scheduling who is using the software license when, issues regarding the computer mirroring software, errors with conservation of charge and current directionality, and difficulty setting the mesh size.

4.1: Simulating the Coil with the Magnetic Field

My first attempt to simulate the coil was a more advanced simulation in which I imported the CAD file of the wire coil into COMSOL, added current to the wires, and attempted to run the simulation. This first simulation failed due to the model being too complicated, with the simulation trying to account for the space between the wires of the top and bottom parts of the coil, as shown in Fig. 3.1.

The second attempt at the COMSOL simulation of the spin dressing magnet was to create a significantly more simple model. Instead of using a coil of wires at the top and bottom of the model, I instead made a cylinder using the shape builder and I made individual drop-down lines in the placement of the wires using the measurements of the wire slots taken with the ROMER arm. These drop-down lines intersect the edges of the cylinder, making smaller curves that can be individually selected. Each drop-down wire was assigned a current of 1 amp in the appropriate direction, as shown in Fig. 3.2. The curved portions of the cylinder edges were assigned appropriate corresponding currents such that the aggregate current across that segment would match the number of n wires in a coil at that part of the magnet. It took some time to properly assign the current values to their spots, as both the directionality of the current and conservation of charge needed to be accounted for.

Once the cylinder was completed, a small rectangle was constructed inside of the cylinder to be the area over which the data needed to be taken, and a larger rectangle was constructed outside the cylinder to be the boundary conditions. The

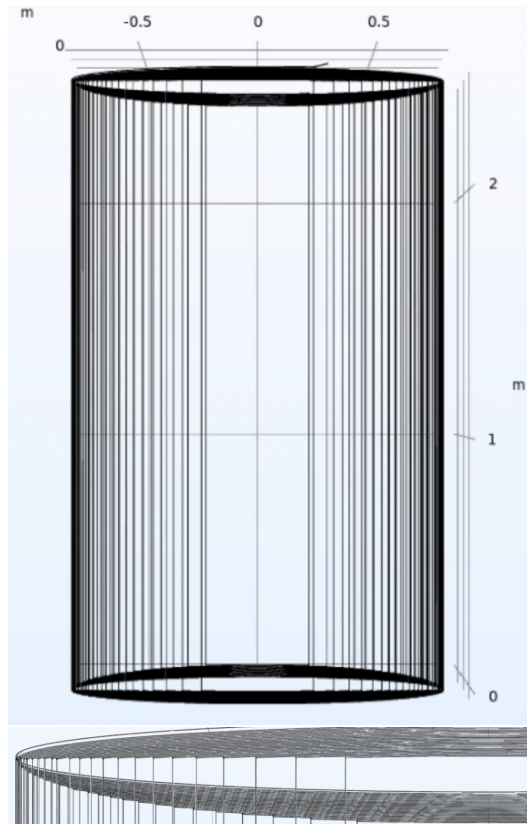


Figure 3.1: Two images, showing the regular (top) and zoomed in (bottom) coil from the original COMSOL simulation. As shown in the bottom image, there are tiny gaps between the wires making up circular portion of the coil, which made the simulation impossible to run on a reasonable time scale.

system was then meshed, during which a problem occurred. Finding the correct mesh size became rather difficult and took several attempts. Each part of the simulation required a different mesh size, and eventually the "finer" mesh size worked. Furthermore, to make it more simple, the simulation was reduced to one quarter of the full size, and extrapolations would be made using symmetry, as the cylinder is symmetric across the x- and y-axes. Figure 23 shows the model with and without the mesh. The mesh size on the inside of the cylinder, where it is darkest in Fig. 3.3, is 0.03 m in size, while elsewhere the size is the preset "finer" size.

4.2: Graphing the Simulation Results

With the Figures 3.4 through 3.6 show different measurements of the magnetic field and its gradient across the quarter of the cylinder. As shown in Fig. 3.4 through 3.6, the magnetic field in the x-direction (B_x) can be approximated by a

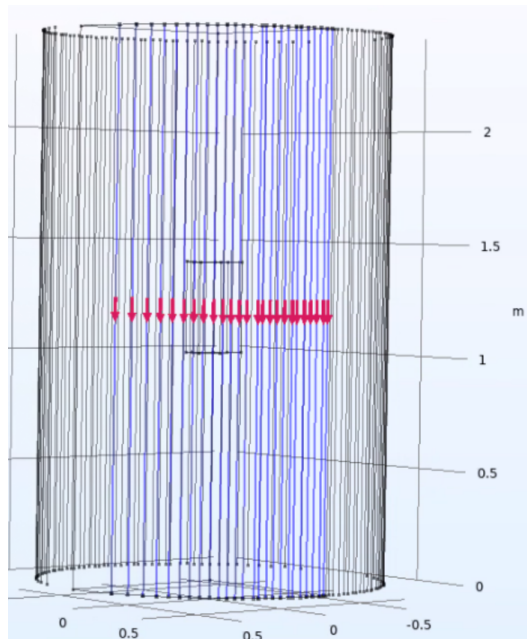


Figure 3.2: An image showing the second iteration of the COMSOL simulation, specifically highlighting the current directionality of the 1 Amp drop-down wires of the cylinder by the blue highlighted lines with the red arrows.

parabola. This was to be expected, with the B_x in a parabolic curve. The average value for the B_x in the x-direction and B_x in the y-direction are 0.213 G. The theoretically predicted value, predicted by Professor Brad Filippone, is 0.223 G, which was predicted by averaging over a finite number of Biot-Savart predictions.

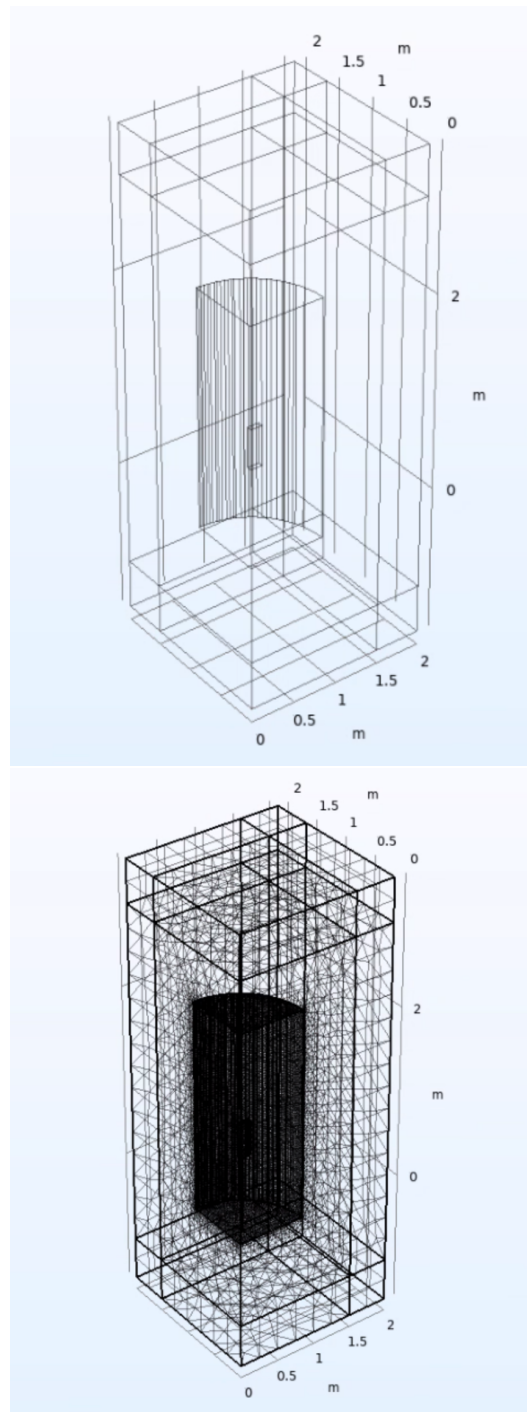


Figure 3.3: An image of the finished COMSOL simulation, both without (top) and with (bottom) the mesh. Inside the coil is a small box, showing the area over which the simulation matters most.

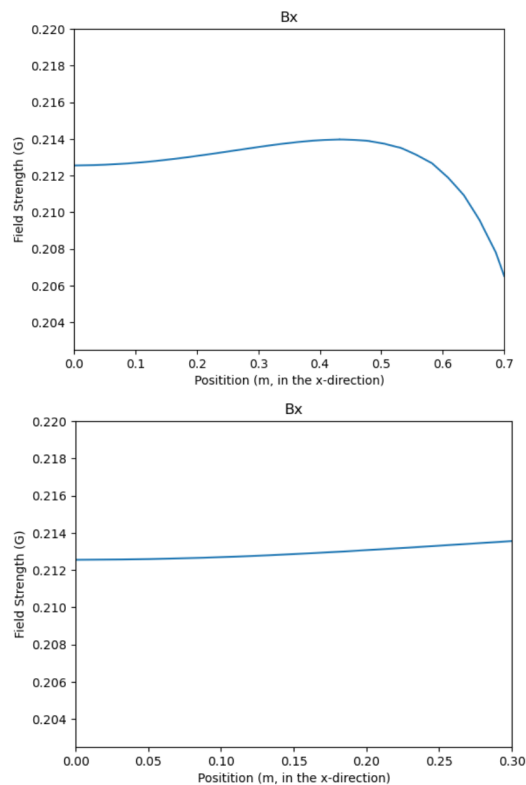


Figure 3.4: A graph of the magnetic field in the x-direction with respect to the x-axis coordinates of the magnet, with the x-axis direction shown in Fig. 1.3. The right side of the graph is the edge of the cylinder, at 0.7m, while the left side is the center of the cylinder, at 0m. Though this is only one quarter of the cylinder, it shows half of the x-axis data and, due to the symmetry of the cylinder, it can be concluded that the data from the other half of the cylinder is the data shown reflected across the y-axis. The magnetic field at the center in this direction is 0.213 G (which agrees with the other two measurements), compared to the 0.223 G calculated by Professor Brad Filippone.

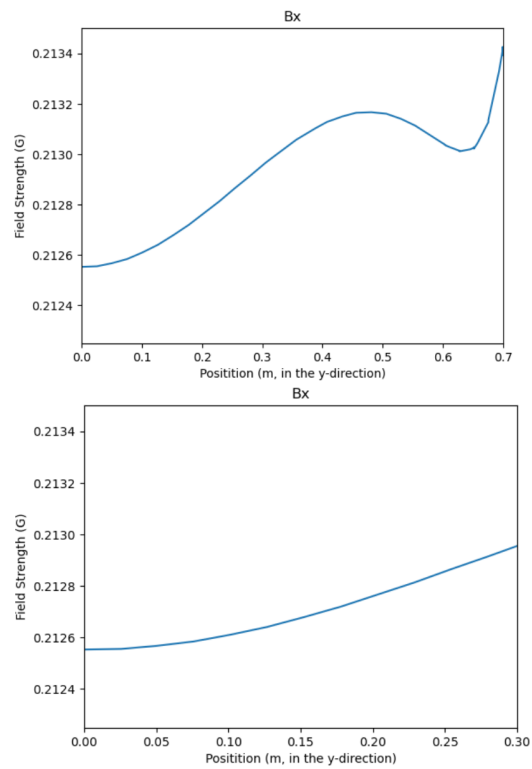


Figure 3.5: A graph of the magnetic field in the x-direction with respect to the y-axis of the magnet, with the direction of the y-axis shown in Fig. 1.3. The center of the magnet is marked by the origin of the graph's x-axis, with a value of .213 Gauss, which agrees with the other two measurements.

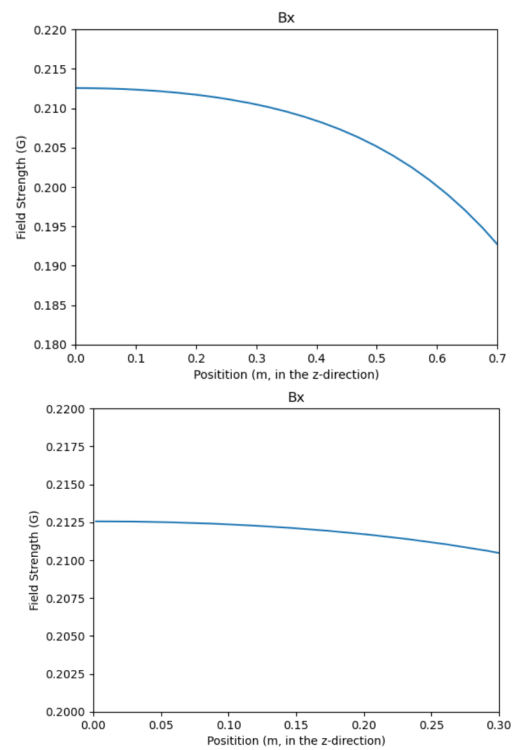


Figure 3.6: A graph of the magnetic field in the x-direction with respect to the z-axis of the magnet, with the direction of the z-axis shown in Fig. 1.3. The center of the magnet is marked by the origin of the graph's x-axis, with a value of .213 Gauss, which agrees with the other two measurements.

Chapter 4

TESTING THE SPIN DRESSING MAGNET

In order to measure the magnetic field of the magnet, first, it had to be ensured that there was no ferromagnetic material being used inside of the magnet. Hence, all materials inside the magnet for the measurements, made of G10, aluminum, or other nonferromagnetic materials. To create the magnetic field, a power supply (shown in Fig. 4.1, along with the magnetometer) supplied one amp into the wire. For measuring the magnetic field, the measurements were taken using a Mag03 Fluxgate magnetometer from Borington (Fig. 4.2). This probe from the magnetometer was placed on a ruler which, in turn, laid across the hoops, as shown in Fig. 4.3. In order to take the data, the probe was moved linearly across the ruler to different positions at 4-inch intervals, both with the current on and off, in the x and y-directions, and at each position, the magnetic field was recorded. For the z-direction, the ruler was rested against the top and bottom of each of the hoops, as well as along the top of the bottom LEC. Near the center of the magnet, data was taken multiple times, and every few measurements, the current of the wire was recorded so that any change could be accounted for.

For plotting the data, only the magnetic field in the x-direction was plotted, as that was what was later done in the simulation as well. The values plotted were the values of the data without the current on subtracted from the magnetic field values with the current on, to account for the Earth's magnetic field. The graph for the x-axis (Fig. 4.4) is of a similar shape (though it shows the full magnet and not just half of the magnet) to the corresponding simulation graph (Fig. 3.4), and has similar values, with a magnetic field value near the center of 0.211 G. For data taken in the y-direction of the magnet (Fig. 4.5), the shape is not as similar to the expected values of Fig. 3.5 on the left half of the graph, though the right half is much more similar. It had a value closest to the center of 0.211 G. Much like the data collected in the magnet's x-direction, the magnetic field values are similar to the predicted values of the simulation. In the magnet's z-direction (Fig. 4.6), the data is also very similar to that of the values predicted in Fig. 3.6, with a center value of 0.210 G. For all the data, the error was approximately 3.79 mG.



Figure 4.1: A photo of the power supply (top right), as well as the ammeter (top left) and magnetometer readout (middle left) used for taking the data of the magnetic field. The other two devices in the photo are non-functional power supplies.

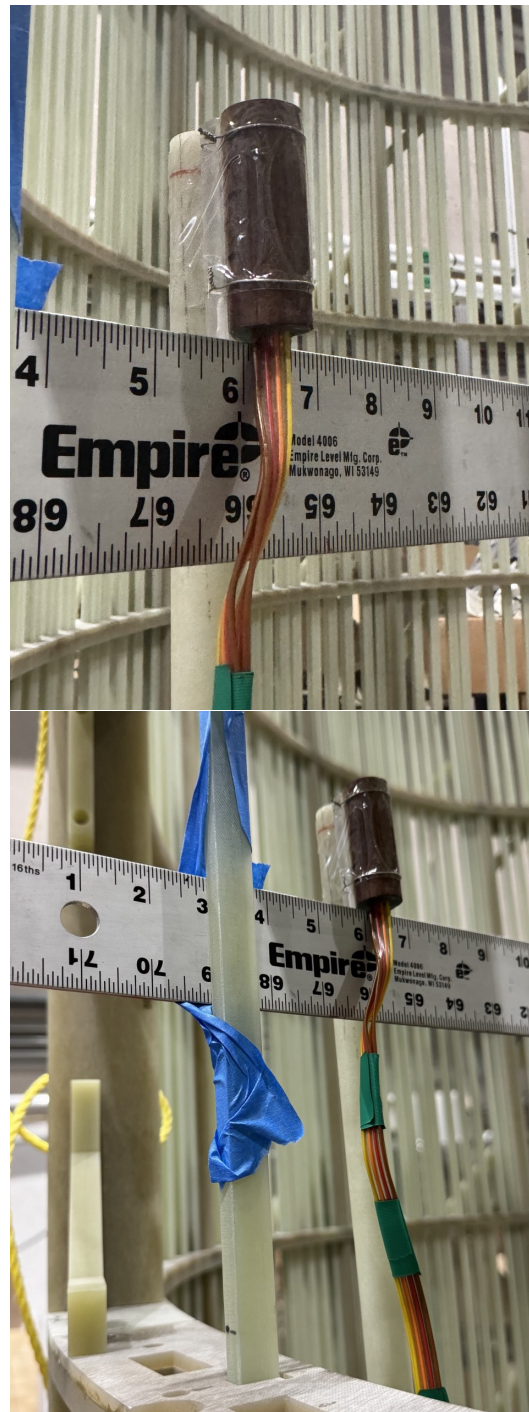


Figure 4.2: Two photos, at varying distances, of the magnetometer probe. The zoomed out image also shows some of the experimental setup. Attached to the probe was a short G10 rod to keep the probe balanced.



Figure 4.3: A photo of the experimental setup, showing the ruler across the x-axis of the spin dressing magnet, with the probe resting on the magnet.

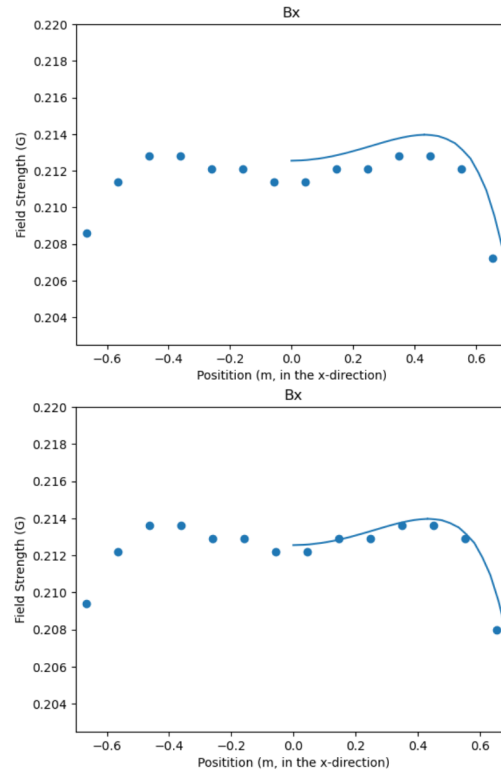


Figure 4.4: A graph (top) of both the simulated (line) and experimental (dots) data of the magnetic field in the x-direction taken across the x-axis of the spin dressing magnet. The shape of both sets of data are incredibly similar, even though the experimental values are less than the simulated values. The bottom graph shows the data normalized, with a normalization factor of 0.000799, which is close to the 0.05% error from the magnetometer.

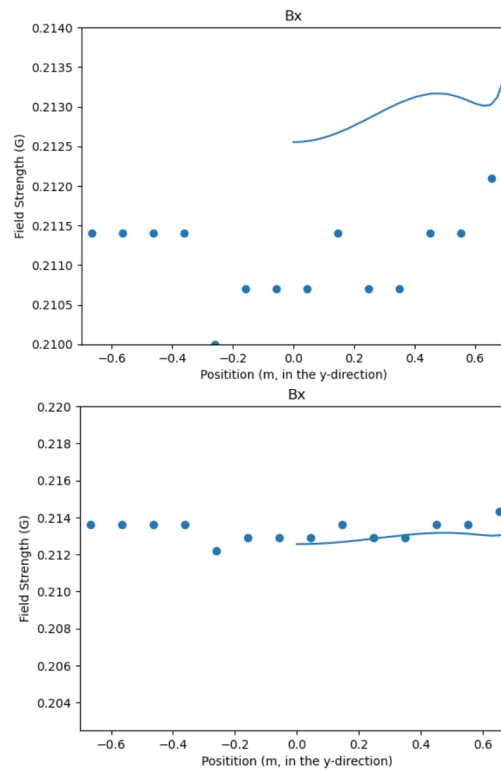


Figure 4.5: A graph (top) of both the simulated (line) and experimental (dots) data of the magnetic field in the x-direction taken across the y-axis of the spin dressing magnet. The shape of both the experimental data is somewhat similar to that of the theorized data, however, there are significant differences. The data may look more similar if data was taken at more regular intervals. The bottom graph shows the data normalized, with a normalization factor of 0.00221, which is farther from the 0.05% error from the magnetometer than the measurements of B_x in the x direction measurement.

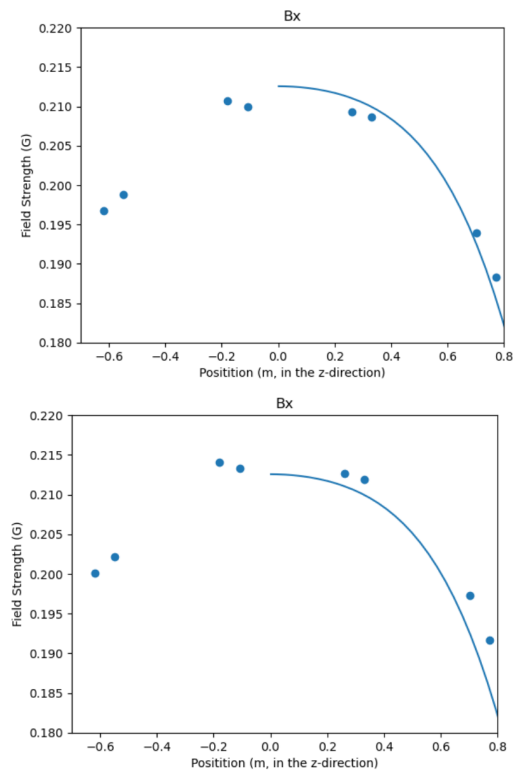


Figure 4.6: A graph (top) of both the simulated (line) and experimental (dots) data of the magnetic field in the x-direction taken across the z-axis of the spin dressing magnet. The shape of both sets of data are incredibly similar, with the experimental values also being similar to simulated values. The two plots would also likely look more similar if experimental data was taken at more regular intervals. The bottom graph shows the data normalized, with a normalization factor of 0.00335, which is farther from the 0.05% error from the magnetometer than either the Bx in the x direction or the Bx in the y direction measurements.

*Chapter 5***FUTURE WORK WITH THE MAGNET**

Once the magnet is complete and tested, it will be transported to Oak Ridge National Lab and installed into the cryostat that contains the experiment. For this testing, the magnetic field profile of the spin dressing magnet will be measured with both the magnet and the lead shielding below superconducting temperatures, as that is the environment in which the spin dressing magnet will be when searching for the neutron electric dipole moment. Long-term, the members of the nEDM experiment are working with their colleagues in Europe in effort to move the experiment to the European Spallation Source in Lund, Sweden.

Chapter 6

CONCLUSION

The construction of the spin dressing magnet was an endeavor that took several months and involved multiple steps, from assembling the individual pieces that comprise the frame of the magnet, to constructing the frame itself, to coiling the wire. For it, the author had to learn how to properly work with G10 and epoxy glue, as well as the safety necessary for working with lead, and how to construct a $\cos\theta$ magnet coil. The most difficult portion of the construction of the spin dressing magnet was not the construction of the magnet itself, but instead, the simulation.

As mentioned above, the author had great trouble setting up the simulation for the spin dressing magnet in COMSOL. These struggles included difficulty coordinating time to use the software, the software not functioning, and issues with understanding the software itself. Though the author of this paper has had previous experience with COMSOL multiphysics, the previous project done was a much simpler coil. As a result, due to those reasons and the struggles with the software, the COMSOL simulation took much longer than expected. However, once the simulation was completed, the results from the simulation matched up with the predicted results with only a 4.5% difference in the x and y-directions, thus a measured magnetic field of a similar value can be expected.

The data taken in the experimental, data collecting portion of the construction of the spin dressing magnet is promising, with values within 0.005 of the simulated data. Furthermore, the magnetic field at the center is only 0.012, 0.012, and 0.013 off from the value predicted by Professor Filippone in the x, y, and z-directions respectively. From this, it can be said that the magnet is working as expected, and the research group, after checking results, can move onto the next phase of the nEDM experiment.

BIBLIOGRAPHY

- [1] Golub, R., & Lamoreaux, K. (1993). Neutron Electric-Dipole Moment, Ultracold Neutrons And Polarized ^3H . https://www.sciencedirect.com/science/article/pii/0370157394900841?ref=pdf_download&fr=RR-2&rr=93978b950b30d12a
- [2] Leung, K. K. H., & et. al. (2019). The neutron electric dipole moment experiment at the Spallation Neutron Source. <https://arxiv.org/abs/1903.02700>
- [3] Sun, X. (2022). Measurements of Beyond Standard Model Interactions with the UCNA and nEDM@SNS Experiments. https://thesis.library.caltech.edu/14440/1/Thesis_XuanSun_December_2021_FINAL.pdf
- [4] Ahmed, M W, et al. “A New Cryogenic Apparatus to Search for the Neutron Electric Dipole Moment.” *Journal of Instrumentation*, vol. 14, no. 11, 13 Nov. 2019, pp. P11017–P11017, arxiv.org/pdf/1908.09937, <https://doi.org/10.1088/1748-0221/14/11/p11017>. Accessed 17 Oct. 2024

*Appendix A***WIRE PLACEMENTS**

A plot of the wire measurements, both relative to each other (center column) and relative to the starting point (right column).

Slot number	Nominal angle position	Angle position
l1	16.84523 [DEG]	16.84523
l2	16.84523 [DEG]	33.69046
l3	6.1798 [DEG]	39.87026
l4	5.2499 [DEG]	45.12016
l5	4.44322 [DEG]	49.56338
l6	3.97102 [DEG]	53.5344
l7	3.59803 [DEG]	57.13243
l8	3.15579 [DEG]	60.28822
l9	3.11784 [DEG]	63.40606
l10	3.11904 [DEG]	66.5251
l11	2.99491 [DEG]	69.52001
l12	2.5124 [DEG]	72.03241
l13	2.5757 [DEG]	74.60811
l14	2.44668 [DEG]	77.05479
l15	3.59895 [DEG]	80.65374
l16	1.44804 [DEG]	82.10178
l17	2.50201 [DEG]	84.60379
l18	2.31434 [DEG]	86.91813
l19	2.56313 [DEG]	89.48126
l20	2.70915 [DEG]	92.19041
l21	1.6242 [DEG]	93.81461
l22	2.72138 [DEG]	96.53599
l23	2.27822 [DEG]	98.81421
l24	2.38028 [DEG]	101.19449
l25	2.69374 [DEG]	103.88823
l26	1.82081 [DEG]	105.70904
l27	2.27241 [DEG]	107.98145
l28	1.82081 [DEG]	109.80226
l29	2.69374 [DEG]	112.496
l30	2.38028 [DEG]	114.87628
l31	2.27822 [DEG]	117.1545
l32	2.72138 [DEG]	119.87588
l33	1.6242 [DEG]	121.50008
l34	2.70915 [DEG]	124.20923
l35	2.56313 [DEG]	126.77236
l36	2.31434 [DEG]	129.0867
l37	2.50201 [DEG]	131.58871
l38	1.44804 [DEG]	133.03675
l39	3.59895 [DEG]	136.6357
l40	2.44668 [DEG]	139.08238
l41	2.5757 [DEG]	141.65808
l42	2.5124 [DEG]	144.17048
l43	2.99491 [DEG]	147.16539

l44	3.11904 [DEG]	150.28443
l45	3.11784 [DEG]	153.40227
l46	3.15579 [DEG]	156.55806
l47	3.59803 [DEG]	160.15609
l48	3.97102 [DEG]	164.12711
l49	4.44322 [DEG]	168.57033
l50	5.2499 [DEG]	173.82023
l51	6.1798 [DEG]	180.00003
l52	16.84523 [DEG]	196.84526
l53	16.84523 [DEG]	213.69049
l54	6.1798 [DEG]	219.87029
l55	5.2499 [DEG]	225.12019
l56	4.44322 [DEG]	229.56341
l57	3.97102 [DEG]	233.53443
l58	3.59803 [DEG]	237.13246
l59	3.15579 [DEG]	240.28825
l60	3.11784 [DEG]	243.40609
l61	3.11904 [DEG]	246.52513
l62	2.99491 [DEG]	249.52004
l63	2.5124 [DEG]	252.03244
l64	2.5757 [DEG]	254.60814
l65	2.44668 [DEG]	257.05482
l66	3.59895 [DEG]	260.65377
l67	1.44804 [DEG]	262.10181
l68	2.50201 [DEG]	264.60382
l69	2.31434 [DEG]	266.91816
l70	2.56313 [DEG]	269.48129
l71	2.70915 [DEG]	272.19044
l72	1.6242 [DEG]	273.81464
l73	2.72138 [DEG]	276.53602
l74	2.27822 [DEG]	278.81424
l75	2.38028 [DEG]	281.19452
l76	2.69374 [DEG]	283.88826
l77	1.82081 [DEG]	285.70907
l78	2.27241 [DEG]	287.98148
l79	1.82081 [DEG]	289.80229
l80	2.69374 [DEG]	292.49603
l81	2.38028 [DEG]	294.87631
l82	2.27822 [DEG]	297.15453
l83	2.72138 [DEG]	299.87591
l84	1.6242 [DEG]	301.50011
l85	2.70915 [DEG]	304.20926
l86	2.56313 [DEG]	306.77239
l87	2.31434 [DEG]	309.08673

l88	2.50201 [DEG]	311.58874
l89	1.44804 [DEG]	313.03678
l90	3.59895 [DEG]	316.63573
l91	2.44668 [DEG]	319.08241
l92	2.5757 [DEG]	321.65811
l93	2.5124 [DEG]	324.17051
l94	2.99491 [DEG]	327.16542
l95	3.11904 [DEG]	330.28446
l96	3.11784 [DEG]	333.4023
l97	3.15579 [DEG]	336.55809
l98	3.59803 [DEG]	340.15612
l99	3.97102 [DEG]	344.12714
l100	4.44322 [DEG]	348.57036
l101	5.2499 [DEG]	353.82026
l102	6.1798 [DEG]	360.00006